

AD _____

Award Number: DAMD17-98-1-8157

TITLE: A Low-Cost, High Quality MRI Breast Scanner Using
Prepolarization

PRINCIPAL INVESTIGATOR: Albert Macovski, Ph.D.

CONTRACTING ORGANIZATION: Stanford University
Stanford, California 94305-3027

REPORT DATE: October 2000

TYPE OF REPORT: Annual

PREPARED FOR: U.S. Army Medical Research and Materiel Command
Fort Detrick, Maryland 21702-5012

DISTRIBUTION STATEMENT: Approved for public release
distribution unlimited

The views, opinions and/or findings contained in this report are those of the author(s) and should not be construed as an official Department of the Army position, policy or decision unless so designated by other documentation.

20010521 087

REPORT DOCUMENTATION PAGE			Form Approved OMB No. 0704-0188	
Public reporting burden for this collection of information is estimated to average 1 hour per response, including the time for reviewing instructions, searching existing data sources, gathering and maintaining the data needed, and completing and reviewing the collection of information. Send comments regarding this burden estimate or any other aspect of this collection of information, including suggestions for reducing this burden, to Washington Headquarters Services, Directorate for Information Operations and Reports, 1215 Jefferson Davis Highway, Suite 1204, Arlington, VA 22202-4302, and to the Office of Management and Budget, Paperwork Reduction Project (0704-0188), Washington, DC 20503.				
1. AGENCY USE ONLY (Leave Blank)	2. REPORT DATE October 2000	3. REPORT TYPE AND DATES COVERED Annual (1 Oct 99 - 30 Sep 00)		
4. TITLE AND SUBTITLE A Low-Cost, High Quality MRI Breast Scanner Using Prepolarization		5. FUNDING NUMBERS DAMD17-98-1-8157		
6. AUTHORS Albert Macovski, PhD				
7. PERFORMING ORGANIZATION NAME(S) AND ADDRESS(ES) Stanford University. Stanford, California 94305-3027 macovski@lad.stanford.edu		8. PERFORMING ORGANIZATION REPORT NUMBER		
9. SPONSORING / MONITORING AGENCY NAME(S) AND ADDRESS(ES) U.S. Army Medical Research and Materiel Command Fort Detrick, Maryland 21702-5012		10. SPONSORING / MONITORING AGENCY REPORT NUMBER		
11. SUPPLEMENTARY NOTES				
12a. DISTRIBUTION / AVAILABILITY STATEMENT Approved for public release, distribution unlimited.			12b. DISTRIBUTION CODE	
13. ABSTRACT (Maximum 200 words) Magnetic Resonance Imaging (MRI) has been shown to be more sensitive and equally specific when compared to x-ray mammography for detecting breast cancer. MRI is non-invasive, completely non-toxic, and requires no uncomfortable breast compression. But an x-ray mammogram costs about \$100 whereas an MRI study costs about \$1500. The exam cost is related to the scanner's manufacturing cost (about \$400,000) and sale price (about \$1 to \$3 Million). X-ray mammography units cost about one tenth of the cost of an MRI scanner. Our objective is to tailor a new concept in MRI called Prepolarized MRI (PMRI) for low-cost MR mammography. PMRI substitutes two inexpensive pulsed magnets for the expensive superconducting magnet. We believe that a high-quality MRI breast scanner using prepolarization could be manufactured for less than \$45,000. This project could potentially make MRI as affordable as x-ray mammography. We have made considerable progress this year in realizing a working PMRI scanner. Indeed, we recently obtained our first in vivo human wrist images with our 0.4 T prototype scanner. While the image quality of our prototype scanner is not yet of clinical quality, the results are very promising considering the total cost of the magnets was less than \$30,000.				
14. SUBJECT TERMS Breast Cancer.			15. NUMBER OF PAGES 23	
			16. PRICE CODE	
17. SECURITY CLASSIFICATION OF REPORT Unclassified.	18. SECURITY CLASSIFICATION OF THIS PAGE Unclassified.	19. SECURITY CLASSIFICATION OF ABSTRACT Unclassified.	20. LIMITATION OF ABSTRACT Unlimited.	

FOREWORD

Opinions, interpretations, conclusions and recommendations are those of the author and are not necessarily endorsed by the U.S. Army.

☒ Where copyrighted material is quoted, permission has been obtained to use such material.

☒ Where material from documents designated for limited distribution is quoted, permission has been obtained to use the material.

☒ Citations of commercial organizations and trade names in this report do not constitute an official Department of Army endorsement or approval of the products or services of these organizations.

Does Not
Apply ☐ In conducting research using animals, the investigator(s) adhered to the "Guide for the Care and Use of Laboratory Animals," prepared by the Committee on Care and use of Laboratory Animals of the Institute of Laboratory Resources, national Research Council (NIH Publication No. 86-23, Revised 1985).

☒ For the protection of human subjects, the investigator(s) adhered to policies of applicable Federal Law 45 CFR 46.

Does Not
Apply ☐ In conducting research utilizing recombinant DNA technology, the investigator(s) adhered to current guidelines promulgated by the National Institutes of Health.

Does Not
Apply ☐ In the conduct of research utilizing recombinant DNA, the investigator(s) adhered to the NIH Guidelines for Research Involving Recombinant DNA Molecules.

Does Not
Apply ☐ In the conduct of research involving hazardous organisms, the investigator(s) adhered to the CDC-NIH Guide for Biosafety in Microbiological and Biomedical Laboratories.

Albert Macovski 10/31/2000

PI - Signature

Date

4 Table of Contents

1. Front Cover	1
2. Standard Form 298 Documentation Page	2
3. Foreword	3
4. Table of Contents	4
5. Introduction	4
6. Body	4
7. Key Research Accomplishments	18
8. Reportable Outcomes	20
9. Conclusions	21
10. References	21

5 Introduction

The objective of this research is to develop a new concept in magnetic resonance imaging called Prepolarized MRI (PMRI) for low-cost MR mammography. Although MRI has been shown to be useful for the noninvasive diagnosis of breast cancer, x-ray mammography remains dominant because a typical MRI study costs more than ten times as much as an x-ray mammogram. We believe that a high-quality MRI breast scanner using our new concept of prepolarization could be manufactured for less than \$50,000, which is about 10% of the manufacturing cost of a conventional MRI scanner.

Breast imaging presents several unique technical challenges for the PMRI concept. First, we must accommodate the patient's torso into the magnet configuration. Second, since breast tissue is relatively nonconductive we will need to use extremely sensitive receiver coils to obtain optimal image quality. Finally, we will need to develop PMRI pulse sequences that suppress fat and provide high quality 3D images.

We have made significant progress toward the goal of a prepolarized MRI scanner for human breast imaging. Last month, we made our first *in vivo* human prepolarized MRI image with a 0.4 T polarizing magnet and a 22 mT readout magnet. While our images are not yet of clinical quality, this breakthrough is very encouraging for the development of a prepolarized MRI breast scanner. Below we detail this year's progress.

6 Body

The diagram in Fig. 1 shows our first prepolarized MRI prototype scanner, a 5-cm-bore system that can be pulsed to 0.5 T at 100 A and uses a readout field of 22 mT (or a 1 MHz center frequency). We will refer to this as the 5-cm-bore prototype. We used a 20-cm-bore Go-

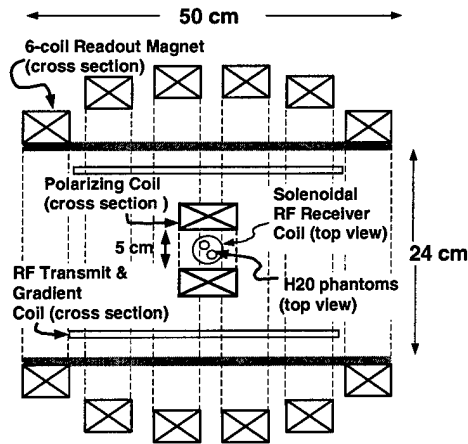


Figure 1: Sketch of our prototype 5-cm-bore prepolarized MRI scanner. The strong (0.5 T) polarizing magnet is coaxial with and inside the low-field (25 mT, or 1 MHz NMR frequency) readout magnet. The magnets and power supplies cost less than \$30,000 in capital costs.

lay gradient set, a 22-cm-bore saddle RF transmit coil, and a 3-cm-bore solenoidal RF receive coil. The unique subsystems of our PMRI system are described below in greater detail.

In this section, we show the results of our experiments demonstrating our ability to increase the SNR in both NMR free induction decay (FID) signals as well as in MR images. We then show that the available contrast using prepolarized MRI is similar to, and in principle richer than, standard MRI. Finally we discuss the individual components of the system and how we have assembled them into a working PMRI scanner that has been used to collect *in vivo* human MR images of the hand.

6.1 PMRI SNR Studies

In principle, a prepolarized MRI scanner with a 1.0 T polarizing field should offer the SNR and contrast of a conventional 1.0 T MRI scanner, independent of the center frequency for MRI data collection. This is true provided that additional noise sources do not degrade

the image quality, which can happen at very low readout frequencies. In fact, the exact minimum readout frequency depends critically on both the size and conductivity of the tissue sample [1]. To ensure no loss of SNR, the noise induced from the patient's conductive tissue must dominate all other receiver noise sources, including the receiver coil, preamp, and matching network. This is called "body noise dominance," and it is well known that it is difficult to obtain for small samples (e.g., for spectroscopy and microscopy) and at low frequencies [2]. We discuss these issues and show our initial experimental results that demonstrate body noise dominance at frequencies as low as 2.0 MHz in §D.

FID Strength Experiments We would expect a linear increase in the NMR signal as a function of the polarizing magnetic field. To verify this experimentally, we collected a set of free induction decay (FID) curves using a pulse sequence with a variable amplitude polarizing field. The experiment was conducted using a small water phantom doped with CuSO_4 to achieve short relaxation times. Figure 2 shows the 5-cm-bore polarizing magnet and the RF coil used in this PMRI experiment. The polarizing pulse was applied for a duration of 600 ms, several times longer than the phantom T_1 at the highest polarizing field, thereby guaranteeing nearly full sample polarization at the end of the polarizing pulse. The largest polarization pulse applied was 0.58 T. Immediately following the end of the polarizing pulse, a 90-degree RF pulse was applied and the signal was collected under the influence of the readout magnetic field alone. The strength of the readout magnet was set at 1 MHz center frequency during these experiments. For each polarizing field amplitude, the initial magnitude of the resulting FID was recorded.

The results of this experiment are shown in

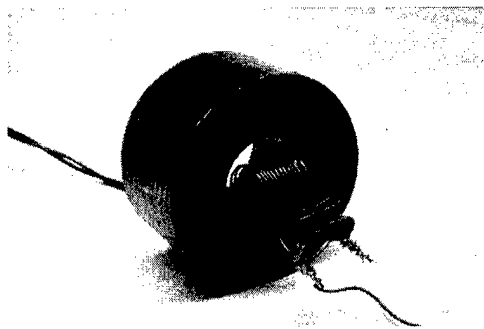


Figure 2: Photo of the experimental setup for the 5-cm-bore PMRI free induction decay (FID) signal amplitude measurements.

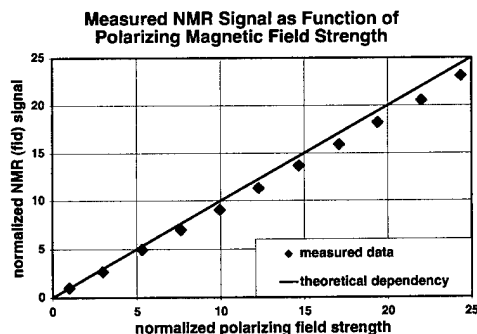


Figure 3: Experimental measurements of the free induction decay (FID) signal amplitude as a function of the applied polarizing field, for a CuSO_4 doped water sample. The axes are normalized to the field and FID signal obtained using the 1 MHz readout field alone. The slope closely matches the theoretical slope of 1.

Fig. 3. The horizontal axis represents the total applied polarizing magnetic field, normalized to the strength of the readout field alone. The vertical axis represents the measured FID signal magnitude normalized to the FID signal obtained with no extra polarizing field applied (*i.e.*, with only the readout magnet creating polarization). The data was fit to a linear curve, yielding an R^2 value of 0.9997. The slope of the fit is 0.94, demonstrating the realization of 94% of the theoretically expected linear increase in signal. This clearly demonstrates that the polarizing field can boost the NMR signal dramatically, in this experiment by a factor of more than 20.

Initial Imaging Results Early this fall we began collecting our first images from the 5-cm-bore prototype system. One of the earliest sets of images is shown in Fig. 4. The two test tubes are approximately 1 cm in diameter and 3 cm deep. The phantoms were two test tubes filled with water doped with copper sulfate. Imaging was performed with a two-dimensional fourier transform (2DFT) sequence with gradient-recalled echoes. Both images were not slice selective. For both images, the effective echo time was 10.2 ms, and the TR was 600 ms, and total imaging time was 51 seconds. The image on the right had a 0.5 T polarizing pulse on during the TR time. Both had a 1 MHz (22 mT) readout frequency. Clearly, the 0.5 T polarizing field greatly increases the SNR of the image on the right, as expected. This was a very encouraging and significant milestone for our project.

To expand our imaging volume, we designed a second generation [3] 13-cm-bore polarizing magnet to fit within the existing 24-cm-bore readout magnet. This polarizing magnet pulses to 0.4 T at 100 A. See Fig. 5 for a diagram. We will refer to this as our wrist-imaging PMRI system.

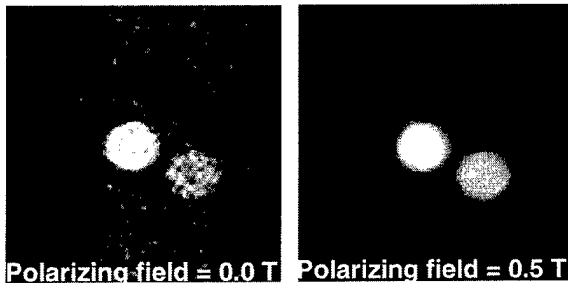


Figure 4: Experimental PMRI image demonstrating the SNR increase by applying a 0.5 T 600 ms polarizing pulse. The FOV for both images is 5 cm, and the matrix size is 64x64, for image resolution of 0.8 mm by 0.8 mm. The readout frequency for both images was 1 MHz. Total imaging time was 51 seconds for both images. Phantom was two test tubes filled with water doped to a $T_1, T_2 = 50$ ms and $T_1, T_2 = 100$ ms.

6.2 Contrast Studies

MRI's excellent soft tissue contrast is based on the differences between T_1 and T_2 relaxation times in diseased and normal states. Both the literature on field relaxometry and our initial experiments confirm that PMRI contrast should be comparable to conventional MRI for the vast majority of human tissues.

Here we show our initial studies on PMRI contrast. We also relate our pulse sequence work designed to optimize contrast for musculoskeletal imaging on a conventional MRI scanner.

6.2.1 Origins of Prepolarized MRI Contrast

The relevant pulse sequence timing intervals that govern the final image contrast are more complicated in PMRI than for normal MRI. The three important intervals are shown in Fig. 6.

First, the build up of longitudinal magnetization is governed by the time-varying T_1 during the polarizing pulse. Although the relaxation process is time-varying due to T_1 dis-

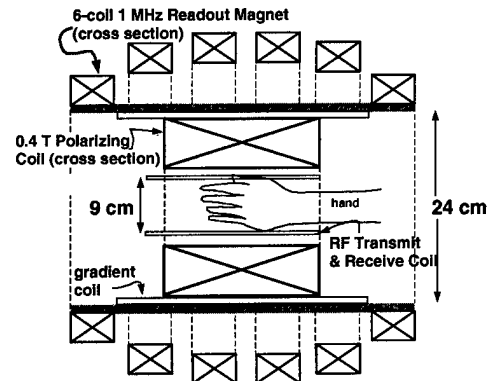


Figure 5: Sketch of our prototype 9-cm-bore prepolarized MRI scanner used for imaging the human wrist *in vivo*. The strong (0.4 T at 100 A) polarizing magnet is coaxial with and inside the low-field (25 mT, or 1 MHz NMR frequency) readout magnet. The total cost of the magnets shown here was also less than \$20,000.

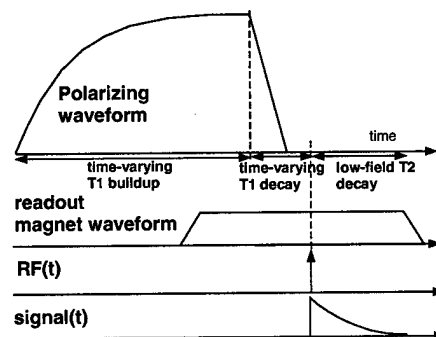


Figure 6: Timing diagram illustrating the different relaxation processes for prepolarized MRI.

persion, this process obtains something very close to high-field T_1 contrast. Hence, short polarizing pulses produce relatively brighter signal from short- T_1 species. As the polarizing pulse ramps down, and before the low-field RF excitation, longitudinal magnetization decays with a time-varying T_1 toward a time-varying equilibrium. After the RF pulse, transverse magnetization decays with low-field T_2 , which is similar to high-field T_2 .

A related issue we studied was the speed of the polarizing magnet rampdown and its effect on the relaxation of the spin system. Using the instantaneous relaxation form of the Bloch equation we found in a simulation study and experiments on the Vahalla hospital field cycling spectrometer [4] that less than 20% of the magnetization was lost if we ramp the polarizing magnet down faster than 80 ms. This is within the FDA dB/dt limits of 20 T/s provided the maximum field is less than 1.6 T.

6.2.2 Prepolarized MRI Contrast Studies

It is well known that the T_1 of biological tissues generally increases with polarizing field strength, whereas T_2 is generally invariant to magnetic field strength. There are a few exceptions, *e.g.* deoxygenated blood T_2 is longer at low field. These variations in relaxation have been measured using field cycling spectrometers, which are the non-imaging precursors to prepolarized MRI. The relaxometry studies include blood [5, 6, 7, 8], gray and white matter [9], liver and skeletal muscle [10], and Bottomley's compendium [11].

Using our wrist-imaging PMRI system, we recently made a measurement of the T_1 variation with field strength for canola oil and chicken muscle. We varied both the duration and the amplitude of the polarizing pulse and recorded the peak strength of the FID signal. We fit the data to an exponential increase in magnetization. We then extracted the T_1 's at ten different field strengths. The results are shown in Fig. 7. The chicken muscle disper-

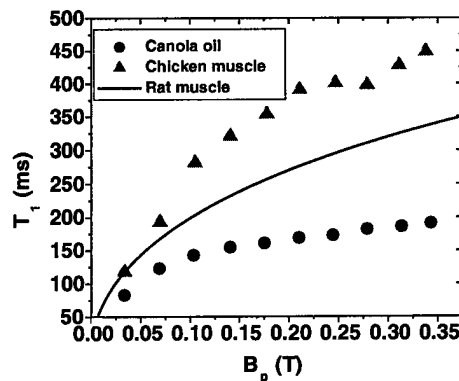


Figure 7: The variation in T_1 with field strength for canola oil and chicken muscle measured on our wrist-sized prepolarized MRI scanner. The solid line is a curve fit to rat muscle T_1 dispersion data from [12].

sion data is also compared in this plot with a data fit for rat muscle tissue from [12]. The chicken muscle and the rat muscle have similar functional dependence, as one might expect. Fig. 8 is a T_1 -weighted scan taken on our 5-cm-bore scanner that demonstrates conventional bright fat signal.

6.3 PMRI Instrumentation

We have built two PMRI systems (the 5-cm-bore system and the wrist scanner), and we now have convincing evidence that prepolarized MRI offers a significant reduction in capital cost relative to a conventional MRI scanner. Table 1 summarizes the capital costs of the unique elements of our two prototype systems.

We also purchased a commercial Tecmag Apollo Low-Field imaging console. This console cost more (\$48,000) than the entire cost of the prototype. We did build an NMR console earlier in the project, so we know that the hardware costs, including the digital RF section, were less than \$2,000 [13, 14]. Hence, we are confident that if PMRI is successful, a much less expensive console could be built.

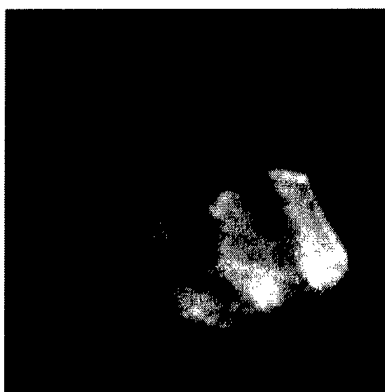


Figure 8: PMRI gradient echo image of a piece of bacon, demonstrating conventional fat-tissue image contrast. The matrix size was 64x64, 5 cm FOV, 780x780 μm in-plane resolution, 23.6 ms effective echo time, no averages, and a total imaging time of 30.1 s. No slice select was applied because the bacon slice was only about 4 mm thick. The polarizing pulse was applied at an amplitude of 0.55 T for 200 ms, allowing for T_1 image weighting. The fat is clearly brighter than the muscle.

Also, the gradient amplifiers are much less expensive than conventional MRI because the PMRI imaging bandwidth is rather low (10 kHz) and the radius of the gradient is small. There also could be significant savings on the RF screening of a PMRI scanner. Other low-field manufacturers (e.g., Esaote) have opted for conductive strips to shield the patient's knee rather than using a complete screen room.

Below we detail the requirements, preferred design, and results for each of our subsystems.

6.3.1 Polarizing Magnet

The purpose of the polarizing magnet is to provide as strong a field as possible given power constraints. Fortunately, the spatial homogeneity requirement is quite relaxed.

Subsystem	5-cm-bore	wrist-scanner
Polarizing Magnet	\$400	\$500
Polarizing Supply	\$750	\$750
Readout Magnet	\$17,000	\$17,000
Readout Supply	\$5,000	\$5,000
Gradient Coils	\$100	\$100
Gradient Amps	\$3,000	\$3,000
Totals	\$26,250	\$26,350

Table 1: Estimates of capital costs itemized for each of our two prototype scanners.

This is because differences in polarizing field strength cause only a corresponding variation in the local magnetization produced in the object. This is equivalent to a difference in proton density, causing only a shading of the image intensity proportional to the inhomogeneity. For this reason, we can use a simple solenoid to generate the field.

To date, we have designed and constructed three polarizing magnets. In general, the inner bore is fixed by the size of the object to be imaged, and the outer bore and length are the two design variables. Our first design was a minimum-power geometry [15] solenoid, in which the outer bore is three times the inner bore and the length is twice the inner bore. These magnets tend to be fairly heavy and somewhat costly. Moreover, very little of the magnet is useful for imaging. Two years ago we developed a "minimum-cost" method for designing solenoids [3]. Here we trade efficiency for dramatically reduced conductor mass. Figure 9 compares the results of the two design methods for wrist-sized polarizing magnets.

Our minimum-cost, wrist-sized polarizing magnet has a 13-cm bore. The outer diameter is 22 cm, and length is 21 cm. At 100 A, it creates 0.4 T field strength, dissipating 10 kW. It has a mass of 42 kg, inductance of 65 mH, and resistance of 1 ohm. This magnet cost only \$500.

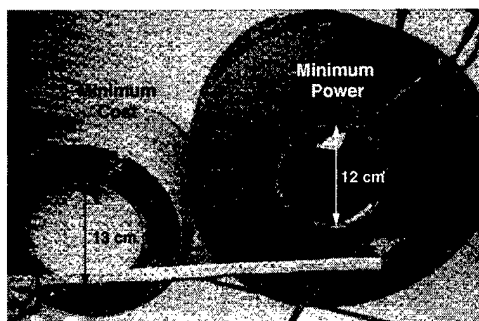


Figure 9: Photograph showing a minimum cost and a minimum power magnet. At 100 A, the minimum power magnet achieves a 0.4 T field, dissipating 10 kW.

6.3.2 Polarizing Magnet Pulsing Circuits

The polarizing magnet supply requires both high power and fast switching electronics. Our wrist-sized coil dissipates 10 kW when operating at 0.4 T. Fortunately, we can tolerate poor current regulation, since the magnetization response time is limited by T_1 to hundreds of milliseconds. The most challenging specification is the current rampdown, which must be under 100 ms to limit unwanted magnetization decay during the rampdown [4]. A field holding several tens of kJ of stored energy must be completely quenched (to less than a few μT) before RF excitation and signal acquisition. Otherwise, the dramatic inhomogeneity of the polarizing field will cause significant MRI signal dephasing.

To satisfy these constraints, we use a power switching circuit which efficiently transfers the coil energy to a capacitor with minimum dissipation in the semiconductor switch. Last year, we built a 100 A polarizing pulsing circuit [16], shown in Fig. 10.

Figure 11 shows a 97 A polarizing coil pulse (0.4 T) and the capacitor voltage. This circuit cost only \$750, most of which was due to the capacitors. This circuit is scalable, extremely robust, and inexpensive.

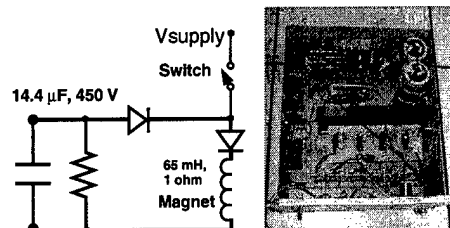


Figure 10: Our pulsing circuit diagram (left) and a photo of the circuit (right).

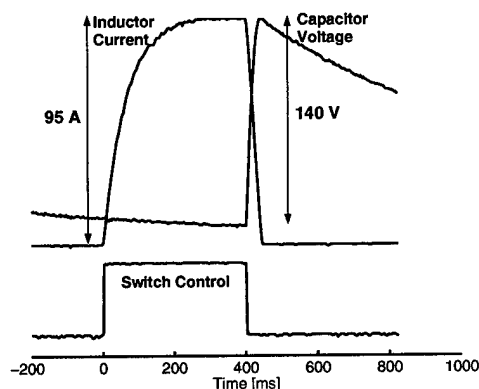


Figure 11: 100 A polarizing pulse (0.4 T) measured with an inductive current probe. Capacitor voltage also rises by 140 V as the stored energy is transferred in 65 ms.

6.3.3 Readout Magnet

Our first readout magnet was designed to create a 50-ppm homogeneous field over the 20-cm DSV (diameter spherical volume). In a compromise between higher readout magnet power and achieving body noise dominance, we chose to operate at a readout frequency of 1 MHz, or 22 mT field strength. The field must be temporally and spatially stable; thermal expansion of the magnet causes a significant downward drift in the resonant frequency.

Our first resistive homogeneous magnet was a variant of the classic 6-coil design [17, 18], with 24-cm diameter free bore and 20-cm spherical homogeneous volume. Figure 12 shows the magnet and the measured field homogeneity. This magnet and its construction were described in our paper, which was selected as a finalist for the ISMRM Rabi Award [19] (see Appendix 2). Total cost for this magnet was \$17,000, mostly due to machining costs. At 1 MHz the 110-kg magnet required a current of 13 A, dissipating approximately 2 kW (about two hair dryers). This magnet was used for all of the prepolarized MRI data shown in this proposal.

6.3.4 Readout Magnet Electronics

Although a readout electromagnet is quite inexpensive, the power supply electronics must meet stringent stability requirements. The electronics must regulate current to within 10 ppm and be tolerant to any induced voltages during the polarizing coil rampdown. The power supply must also be capable of providing high pulsed currents. If the readout magnet is pulsed on only during the 10% data acquisition interval, magnet heating is reduced. Thus, for the same total power, imaging speed can be expanded by using higher pulsed readout fields.

Pulsed Readout Source In our design, we converted two Techron 8607 MRI gradient

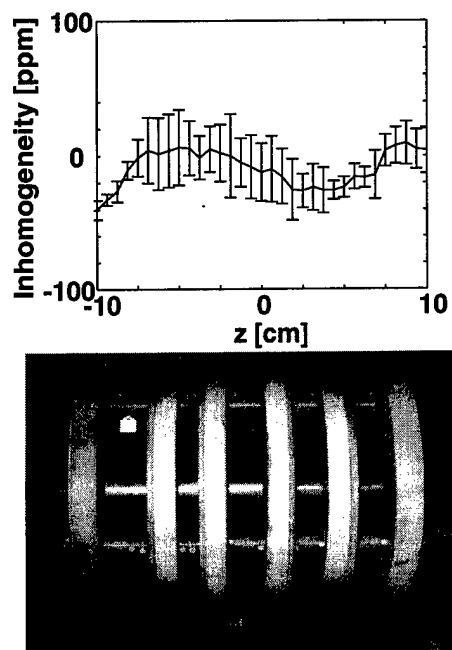


Figure 12: Photo of our \$17,000 homebuilt 24-cm-bore, 23 mT, 2 kW homogeneous magnet for PMRI of extremities. The homogeneity plot indicates 40 ppm uniformity.

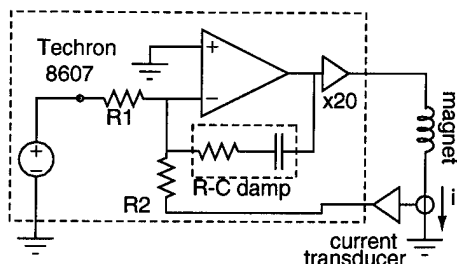


Figure 13: Readout supply using Techron amplifiers, which act like power op-amps. Current is sensed by our precision current transducer, and the RC damp circuit speeds up transient decay. This circuit can pulse our readout magnet to .18 T.

amplifiers operating in a master-slave mode to a pulsed readout current source capable of delivering up to 100 A. From our earlier experience with shunt-regulated magnet current sources [20], we have learned how to use a precision current transducer to achieve over 70 dB improved regulation. The Techron amplifier system is functionally equivalent to an op-amp with a power $\times 20$ output amplifier (see Fig. 13). We modified the control circuit of the master gradient amplifier to sense magnet current with a Danfysik Ultrastab current transducer. Finally, a series resistor-capacitor network in the feedback compensation (RC damp) was adjusted to provide the shortest possible recovery time to pulsed transients.

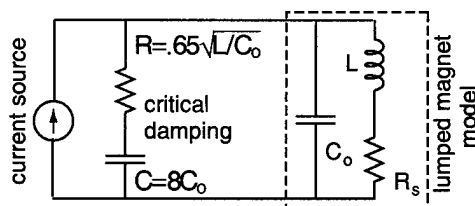


Figure 14: The Techron amplifier acts like a current source with an RC output impedance. The values shown minimize the electromagnet recovery time after prepolarizing pulses.

Critical Damping During rampdown, the voltage induced in the readout coil also disturbs the magnet current. Readout magnet disturbances must decay below ppm levels within 5 ms of the end of the polarizing coil rampdown interval to allow for data acquisition in a homogeneous field. Although our magnet had 11 Ω resistance, giving a DC L/R_s time constant of 35 ms, it is still possible to reduce the time constant below 500 μ s using the critical damping method shown in Fig. 14. The Techron, together with its RC compensation components, acts like an ideal current source with a series RC output impedance. Since a magnet inductor L always has stray capacitance C_0 present, any disturbances cause ringing. The RC values shown cause the exponential decay times to reach the shortest possible time. For our 0.34 H magnet a transient decay time of 226 μ s is possible. Allowing for 14 time constants to guarantee all disturbances fall below ppm levels, we can record FIDs just 5 ms after the rampdown of the polarizing magnet. Before we implemented critical damping, we had to wait nearly 100 ms for the readout magnet transient to settle. This wait severely attenuated the NMR signal.

Figure 15 shows experimental proof of the critical damping. The polarizing rampdown from 50 A (a), and voltages exceeding 50 volts are induced in the readout magnet (b). With critical damping the recovery time is under 5 ms (c), while an underdamped system response is disastrous (d).

6.3.5 RF System

Since prepolarized MRI uses a very low-field readout magnet, signal detection is significantly more challenging than high frequency detection. PMRI requires a high Q receiver coil integrated with a matching network, and preamp optimized for the largest possible SNR and bandwidth. To minimize sensitivity loss from the polarizing coil, an RF shield is also required. The transmitter coil must

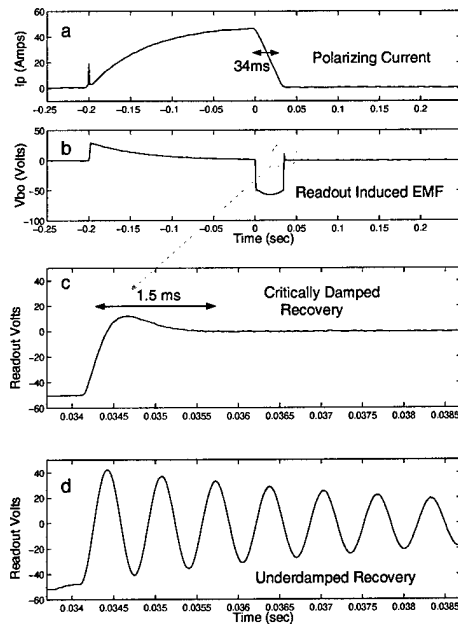


Figure 15: The polarizing current rampdown induces voltage (EMF) in the readout magnet and creates induced currents. A close-in oscilloscope trace at the end of rampdown shows that we can reduce these transients below 5 ms using our critical damping method. Otherwise, transients could remain for over 50 ms, as in the underdamped case.

have a broad bandwidth to minimize distortion of selective RF excitation pulses. For our wrist prototype, we developed a dual mode transmit-receive coil that could achieve these requirements.

High Q Shielded Coils For our wrist prototype, we constructed a 9 cm diameter 4-turn litz saddle receiver coil which had an unloaded Q of 350 at 1.14 MHz. The litz wire, (1725 separately insulated 48 AWG strands) effectively cheats the skin effect and requires less space than copper tube of similar noise performance. The presence of the polarizing coil degraded the Q to 60 without additional RF shielding. After adding a 13 cm slotted copper sheet shield around the 9 cm wrist coil, the unloaded Q exceeded 250 in

the polarizing magnet. The shield slots, located where the wrist coil RF image currents are zero, prevent gradient and polarizing coil eddy currents. The coil and shield are shown in Fig. 16.

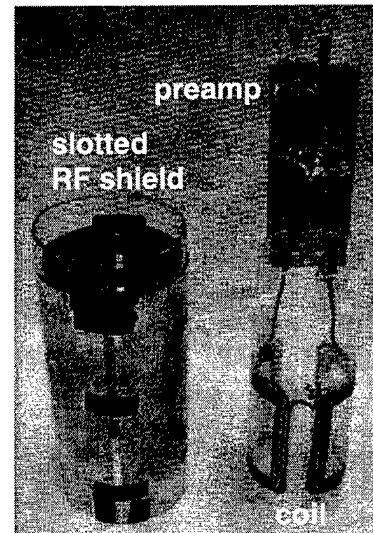


Figure 16: The dual transmit-receive wrist coil is a 4-turn saddle design with a 13 cm diameter slotted shield. The preamplifier is mounted directly on the matching circuit board for best SNR performance.

Transmitter Q-spoiling A low field transmitter coil must have a coil bandwidth exceeding the RF excitation pulse bandwidth. We achieved this by a combination of cross-diode circuits that switch in under high power excitation. For our 5 cm prototype, the crossed diodes of a separate 20 cm transmit-only coil added a series resistance (Fig. 17a). For the wrist imaging system, coil circuits are switched in a parallel resistive load to lower the coil Q, and an LC trap protects the preamplifier without loading the coil (Fig. 17b). The capacitors are adjusted to give 50 Ω input impedance under high power conditions. When RF power is off, the diodes switch off, leaving the receive coil in a high Q, high SNR state.

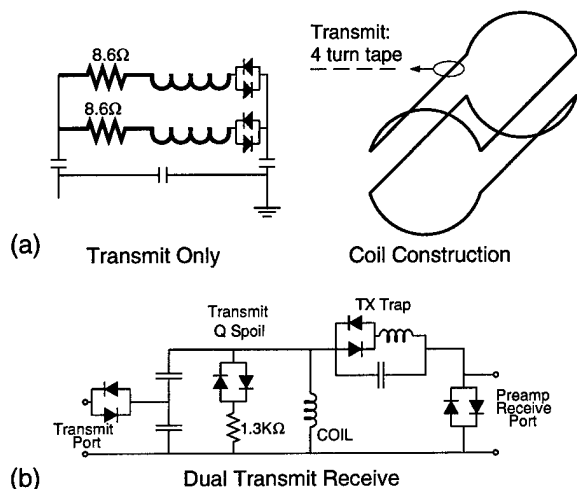


Figure 17: a) The transmit-only coil for our 5 cm prototype uses diode switched series resistors to spoil Q. b) The wrist imaging system transmit receive coil circuit acts as a low Q (17) coil during transmit and a high Q (250) coil during receive. Crossed diodes switch in a Q spoiling resistor parallel to the coil.

Preamplifiers For maximum receiver bandwidth, an ultralow noise preamplifier is crucial. Our first NMR experiments used a variation of a design by Fenzi [21] that employed a feedback resistor to synthesize a low “noiseless” input resistance. This technique flattens the signal (not the SNR) frequency response—a technique typically called feedback damping. The preamplifier was matched to the receive coil at a location that achieves the best overall combination of SNR and bandwidth [22].

Figure 18 shows the wrist coil tuning bandwidth in its transmit, receive, and unloaded modes of operation. We achieve broadened transmit and receive bandwidth suitable for PMRI.

6.3.6 Gradient Design

Like conventional MRI systems, PMRI requires a 3-axis gradient coil to distinguish spin location in space. Because of the small diameter needed for extremities, PMRI does not require

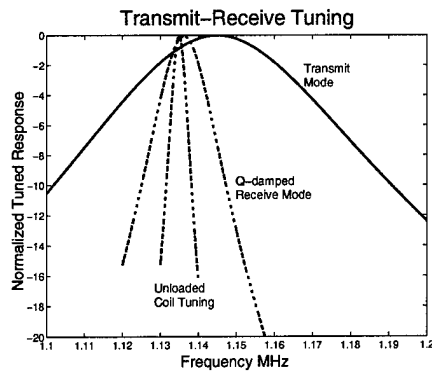


Figure 18: Wrist coil transmit-receive response. In transmit mode (solid), the coil Q is spoiled during high power pulses without distorting the selective pulse shapes. In receive mode (dashed), the preamp damps the Q from its unloaded high Q state (dashed-dot). The received signal is equalized without adding extra noise.

high power gradient coils. For our first gradient coil set, we constructed a simple 3-axis Golay gradient set [23] using inexpensive copper tape layered over an acrylic tube. A photo of the gradient set is shown at the bottom of Fig. 19. At 10 A, we measured 3 mT/m gradient field, which is adequate.

For extremity imaging, the gradient former must be shaped to maximize access and comfort for the limb being imaged. For example, when imaging a knee, it could be important to have the magnet and gradient coil flange out to allow room for the patient's other leg. Most existing fast gradient design algorithms are restricted to conductors lying on a cylinder or a sphere [24, 25, 26]. Hence, we need a more flexible gradient design method. Numerical optimization has been developed for gradients mounted on arbitrary surfaces, but these require excessive computation time [27, 28, 29, 30, 31].

We recently generalized our minimum power homogeneous magnet design to design gradient coils. We discovered that this design

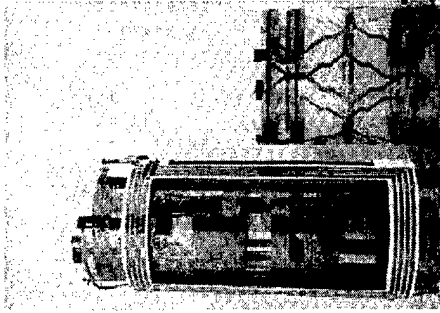


Figure 19: Photograph comparing the length of our minimum power gradient (top) with the classic Golay coil. The Golay set also incorporates transmit and receive coils.

problem can be solved very efficiently with linear programming [32]. Our algorithm has several advantages over existing programs: no approximation is needed to implement the gradient after the design phase, the computation requires less than a minute, the coils typically have less than four loops, the power is minimized, and one can constrain the conductors to an arbitrary surface.

We recently built a constrained length gradient coil for our wrist scanner using this algorithm. The photo in Fig. 19 shows our constrained length gradient is about half as long as the Golay gradient, despite having a larger homogeneous gradient volume. The flexibility provided by this algorithm will help us to design a dedicated extremity scanner.

6.3.7 In Vivo Human Wrist Images

The most relevant test of our PMRI system was the collection of *in vivo* human images. Here we show two representative images to demonstrate our preliminary results. These images were collected using a typical MR pulse sequence (save for the use of switched polarizing and readout magnetic fields), with reasonable acquisition times. The experience was described as comfortable by the volunteer subjects. The images shown are of the

human wrist, expected to be representative of the structures and contrasts in the human knee.

Figure 20 shows an *in vivo* image of an axial slice through the left wrist near the base of the thumb. This gradient-echo image was obtained without averaging. The B_p field was switched on to an amplitude of 0.25 T for a duration of 400 ms prior to RF excitation and subsequent readout of each k-space line, to produce T_1 contrast between fat and muscle tissue. The second through fifth metacarpal bones are readily visualized with bright marrow fat surrounded by dark cortical bone. The flexor tendon group is also apparent. The bright regions in the lower left and upper right of the image are due to RF inhomogeneities, as the wrist was very close to the RF coil windings.

Figure 21 shows a second *in vivo* image of the same volunteer, in this case an axial slice through the wrist at the base of the hand. The imaging parameters are the same as those for Fig. 20, with the exception the B_p pulse was increased to 0.4 T here. Both the flexor and extensor tendons are visible. The phase encode ghosting is discussed in §D.

6.4 Summary

The preliminary studies described above served to test the three fundamental assumptions of prepolarized MRI. First, data was presented indicating the expected linear increase in NMR signal with polarizing field is indeed observed. This fact was also verified in imaging tests where the image SNR improved dramatically with the application of a 0.5 T polarizing field pulse. Second, normal tissue contrast was shown to be attainable with PMRI. T_1 dispersion measurements were carried out and indicated that strong muscle-fat contrast is expected over a full range of polarizing field strengths; furthermore, additional contrast, based on the different dispersion curves of these two typical tissue components, is pos-

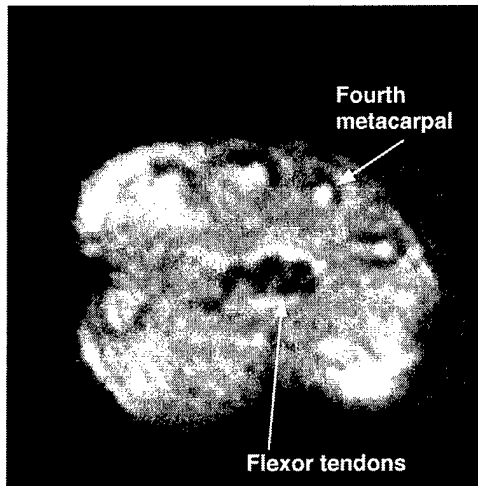


Figure 20: First PMRI *in vivo* image of the human wrist, an axial slice at the base of the thumb. A gradient-echo sequence was used with 64x64 image matrix (zero filled to 256x256), 10 cm FOV, 1 cm slice, 1.56 mm x 1.56 mm in-plane resolution, 12.6 ms echo time, no averages, total scan time of 56.1 s. A polarizing pulse of 0.25 T was applied for 400 ms for T_1 contrast. Phase encode is the horizontal direction. The metacarpal bones and flexor tendons are readily visualized (arrows).

sible. Fat-muscle contrast was also demonstrated in imaging tests of a bacon sample. Finally, two complete PMRI scanners which were built by our group were described in detail and the total capital costs for each system was estimated to be \$26,000. This supports the final and perhaps most important assumption underlying our PMRI project, that the system can be built at an extremely low cost. These positive preliminary results are the motivation for the proposed development of a human breast PMRI scanner.

6.4.1 Receiver Coil Enhancement

A major goal of this program is to make the PMRI sensitivity and imaging speed equivalent to a high field system. The SNR ap-

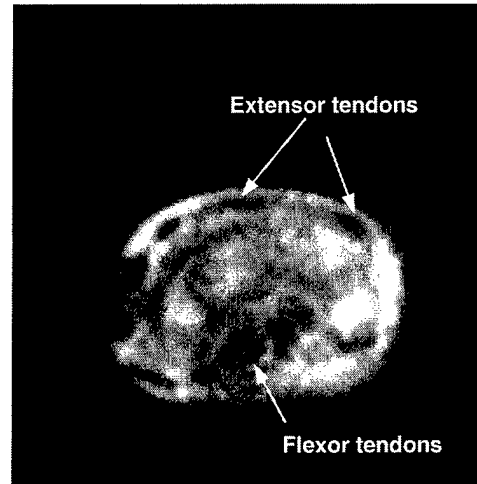


Figure 21: Axial *in vivo* image of the human wrist just proximal to the hand. Pulse sequence parameters were identical to those of Fig. 20. The polarizing pulse was applied at an amplitude of 0.4 T for 400 ms, providing T_1 contrast. Both flexor and extensor tendons are readily visible (arrows).

proaches its intrinsic maximum if over half the received coil noise is dominated by the patient. In fact, tissue conductivity below 4 MHz is only about half that above 50 MHz [33, 34]. Our SNR should be identical to an *ideal* high-field system even if the receiver components contribute half the noise. A design conflict arises because the pulsed readout supply and readout magnet design perform better below 0.1 T (4.3 MHz), but receiver sensitivity and bandwidth improve at higher pulsed fields. Here, our goal is to establish the lowest frequency and coil geometries that give PMRI receiver coils comparable SNR performance to conventional MRI.

Loss Mechanisms and Q The quality, Q , of an RF coil characterizes the total magnetic energy versus losses acting in the resonant circuit. If two coils have the same geometry, the lower Q coil will have higher losses and poorer signal sensitivity. When comparing different

geometries, the ratio of local RF field to coil losses must be compared instead. Each loss mechanism contributes a voltage noise power proportional to its effective resistance in the coil. The main loss mechanisms in MRI coils are coil copper resistance, magnetically coupled tissue loss, and electrically coupled tissue loss [35, 36]. At higher frequencies where the conductor lengths exceed $\lambda/20$, the unloaded Q will drop due to mechanisms such as antenna radiation effects, self-resonance from distributed capacitance, and spatial differences in the phase of coil currents.

Body Noise Dominance Electrically coupled losses can be eliminated with a Faraday shield, and copper losses scale only with the square root of frequency. Inductively coupled tissue losses are tied directly to the RF fields that determine signal strength in NMR and are unavoidable. The inductive losses increase quadratically with readout frequency, and linearly with tissue conductivity. However, tissues typically have twice the conductivity above 50 MHz versus 1 MHz so if exactly half the total noise came from tissue in PMRI, the SNR performance is identical to a high-field system having all noise from tissue. When inductively coupled tissue losses exceed the total of all other losses, we achieve "body noise dominance."

Loaded Q Test Coil Q as a function of frequency was experimentally measured for a 25 cm diameter (*i.e.*, human head sized) solenoid RF coil with and without the presence of a human head loading the coil (Fig. 22). The fraction of noise power due to tissue is plotted as the load factor $L = (1 - Q_L/Q_u)$. Our results, shown in Fig. 23, indicate that patient loading exceeds all other losses above 2 MHz. This is a milestone result, since it indicates that low field reception will cause no significant SNR degradation. The unloaded coil Q reaches an optimum also around



Figure 22: Experimental setup to measure solenoid coil Q with a network analyzer. Patient loading dominated other losses above 2 MHz, indicating that low-field readout will cause no significant loss of SNR.

2 MHz before declining from wavelength effects. With the subject's head inserted into the coil, the coil loading with and without a Faraday shield were similar; hence, electrically coupled tissue losses were not significant.

Tissue Loading Studies: The solenoid study provides a simple baseline measurement with which other coil configurations can be compared. We plan to perform similar Q measurements for saddle, crossed ellipse and other coil geometries and will tabulate their performance for different extremities. The loading studies will also account for sensitivity changes upon cooling or for RF shield proximity. The goal is to determine the best coil, shield and polarizing coil diameters for best overall SNR and power consumption at the lowest readout field.

Flexible Litz Coils We propose to construct flexible litz wire RF coils, which will improve image quality and SNR by fitting the anatomy better. Litz wire cheats the skin effect by braiding separately insulated strands of tiny

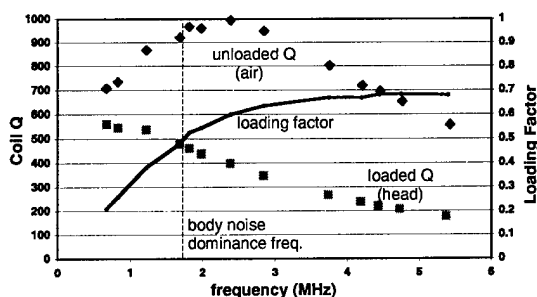


Figure 23: Q measurements demonstrate body noise dominance. The load factor (solid) shows that 50% to 70% of the total losses arise from the human head above 2MHz.

wires. Our 1700 strand 2 mm litz cable is extremely flexible yet has the equivalent RF resistance of 4 to 15 mm copper pipe between 3 and 1 MHz. We will develop both saddle coil and crossed ellipse geometries as receive-only or dual transmit-receive coils using Q-spoil methods already developed. Furthermore, these coils can be arrayed or placed in quadrature with separate preamplifiers to enhance sensitivity. Although the coils are flexible, they will not require precision tuning. Any shift in tuned frequency due to shape changes will be corrected simply by setting the readout magnet B_0 field to the new value.

RF Shields We will minimize RF losses from the gradient and polarizing coils by constructing an RF shield at the largest diameter possible. A shield that is 1.4 times the coil diameter halves the receiver B_1 field but not resistance, so larger diameters or higher receive frequencies will be tested. The shield must mimic a continuous copper sheet at RF, but appear open-circuited for the pulsed gradient and polarizing fields. We will extend our slotted shield design by incorporating large arrays of polypropylene (extremely low series resistance) capacitors across shield gaps to enable RF image currents to flow. Dielectric losses will be removed by a Faraday shield composed of a cage of conductors with no

closed loops.

Cryo-coils If we cool a coil in liquid nitrogen, its resistive noise power will drop by a factor of approximately 10, since copper conductivity also increases at lower temperatures. In effect, a cooled copper pipe or wire has the equivalent noise of a room temperature conductor 10 times larger in diameter. The improved sensitivity can offset shielding effects and allow extra SNR bandwidth. We have already performed preliminary cooling tests of solid 1.5 mm wire versus 1.8 mm diameter litz wire (1725 strand 48 AWG) shown in Fig. 24. Although room temperature litz wire performs well around 1-3 MHz, we can achieve consistently lower noise coils using cooled copper over a wider frequency range above 1 MHz. A copper pipe is well suited

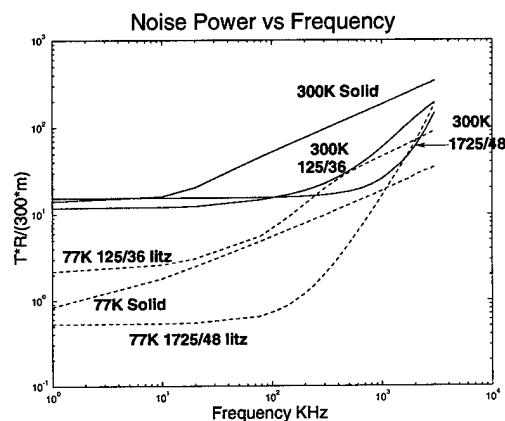


Figure 24: Litz wire (1.8 mm) and solid 1.5 mm wire noise at room and liquid nitrogen temperatures. Within a 1-3 MHz frequency range, room temperature 1725 strand litz performs almost as well as cooled copper wire or 1.5 cm room temperature pipe.

to liquid nitrogen cooling. The nitrogen can be contained in the hollow center of the conductor. Insulation is easy to implement either with styrofoam, or with a PVC plastic vacuum dewar (Fig. 25) similar to [37].

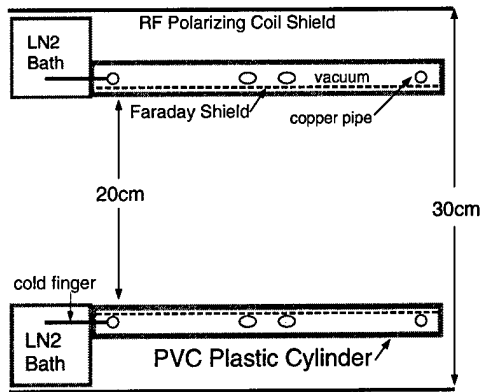


Figure 25: A crossed ellipse or saddle knee coil will be cooled by liquid nitrogen when constructed of copper pipe. PVC tube and a low grade vacuum suffice to protect the patient.

7 Key Research Accomplishments

Our key research accomplishments this year were:

1. Greig Scott and graduate student Nathaniel Matter designed and constructed an ultra-stable switched current supply for controlling the readout magnet. This ultra-precise regulator stabilizes the readout current to better than a 50 parts per million while enabling significantly reduced heating of the readout magnet (due to the reduced duty cycle). The total hardware costs was less than \$1,500. This will be submitted as an abstract to the 2001 ISMRM.
2. We constructed and shimmed a new equi-radius 3 MHz readout magnet with a 30-cm free bore. This magnet has a free bore more than double our hand imaging magnet, and water cooling so that it can operate at 3 times the field strength, or nine times the power. To accommodate these upgrades, we significantly simplified the overall mechanical design by using resistive shims instead of plate-mounted coils.

The magnet cost (\$6,720), which is only 40% of the cost of our hand-sized readout magnet (\$17,000). We were able to shim this magnet to better than 50 ppm on axis. We had two abstracts on this magnet accepted to the 2000 ISMRM.

3. We have modified the linear programming algorithm developed in Year 1 to design shim coils. We are now constructing shim coils to improve the off-axis homogeneity of the 31 cm readout magnet. We will be submitting a shimming abstract to the 2001 ISMRM.
4. Luchin Fay Wong developed our first dual transmit-receive RF coil, which was tested for the hand images shown in the grant. Total hardware cost was less than \$200.
5. Our first experimental demonstration of human body noise dominance at under 2 MHz. This is a key technical verification of the prepolarized MRI concept. Since we have experimentally shown that it is possible to create a pulsed readout field above 3 MHz, we can guarantee no loss of SNR relative to a conventional MRI scanner. We are now preparing an abstract on this to the 2001 ISMRM.
6. First experimental contrast studies, including 1 mm resolution images of bacon, verifying that conventional T1 contrast is obtainable with PMRI. Also measured our first experimental T1 dispersion plots of chicken muscle and canola oil. We plan to submit an abstract to the 2001 ISMRM on this project.
7. We obtained our first phantom carefully demonstrating the linear dependence of signal with polarizing field strength. In fact we were able to increase the SNR by a factor of 24 with a polarizing field of 0.55 T. This will be submitted as an abstract to 2001 ISMRM.

8. First *in vivo* human images of the wrist. This breakthrough will be submitted to the 2001 ISMRM.
9. We found that third-order damping of the readout magnet could greatly reduce transient ringing in the readout field. Without the new damping circuit, the readout magnet would ring for hundreds of milliseconds, rendering our PMRI experiment useless. The readout field is now stable within a few milliseconds of the polarizing magnet rampdown. This new circuit enables PMRI to work.
7. "Concomitant Gradient Effects in Spectral Spatial Pulses," Chi Ming Tsai, Craig Meyer, Steven M. Conolly, Dwight Nishimura, *Proceedings of the ISMRM*, 2000.
8. "A 31 cm Bore Readout Magnet for Pre-polarized MRI" Hao Xu, Steven Conolly, Greig Scott, Albert Macovski, *Proceedings of the 41st ENC, Monterey CA*, poster 180, April 2000.

8 Reportable Outcomes

1. "Homogeneous Magnet Design Using Linear Programming," Hao Xu, Steven Conolly, Greig Scott, Albert Macovski, *IEEE Transactions on Magnetics*, Vol. 36, No. 2, March 2000.
2. S. Mani, G. Luk Pat, S. Conolly, M. Moseley, D. Nishimura, and A. Macovski, "Multiple Inversion Recovery Perfusion," *Accepted by Magn. Reson. Med.*, 2000.
3. "Edge Cooling for Low-Field Homogeneous Magnets," Steven M. Conolly, Hao Xu, Greig C. Scott, Albert Macovski, *Proceedings of the ISMRM*, 2000.
4. "Split Resistive Shimming of Low-Field Homogeneous Magnets," Steven M. Conolly, Hao Xu, Greig C. Scott, Albert Macovski, *Proceedings of the ISMRM*, 2000.
5. "Electromagnetic Criteria for Prepolarization Coils," Greig C. Scott, Steven M. Conolly, Albert Macovski, *Proceedings of the ISMRM*, 2000.
6. "3D Echo Planar DEFT Imaging of Knee Cartilage," B.A. Hargreaves, J.M. Pauly, G.E. Gold, J. Tsai, P.K. Lang, S.M. Conolly, D.G. Nishimura, *Proceedings of the ISMRM*, 2000.
9. Patent Issuance: Steven Conolly, "Minimum-Cost Polarizing Solenoids", pending, filed April 21, 1998. U.S. Patent 6,075,365 granted June 13, 2000. This patent covers a method for constructing a minimum cost polarizing coil for Prepolarized MRI. No effort made yet to commercialize.
10. Patent Issuance: Hao Xu, Steven Conolly, "Method for Designing Electromagnets having Arbitrary Geometrical Constraints," filing date 5/21/99. U.S. Patent 6,067,001, issued May 23, 2000. This patent application describes a general algorithm for designing electromagnets with arbitrary former constraints. We have found this to be very useful for low-cost gradient design, but there has been no effort yet to commercialize.
11. Patent Issuance: Hao Xu, Steven Conolly, Bob Hu "Short Bore-Length Asymmetric Electromagnets for MRI," filed 5/21/99. U.S. Patent 6,064,290. This is a patent for a particular magnet with better patient and physician access. No effort yet to commercialize.
12. This biomedical engineering project has provided undergraduate research opportunities for many undergraduate students at Stanford including Ross Venook,

Dave Pai, Alex Tung, Jack Wang, Serena Wong, Luchin Fay Wong, Karen Tisdale, Jaime Wong, Mike Ross and Lexyne McNealy. Lexyne is a visiting student from Spelman College. The first six students were studying under a Stanford research award called the REU program.

9 Conclusions

We are very encouraged by our recent progress making our first human *in vivo* wrist images on a very low cost MRI scanner. This has been an extremely challenging engineering development. Our initial images are very promising, but certainly not yet of clinical quality. With the continuing support of the Army BCRP program, we believe we can greatly improve PMRI image quality for breast imaging. We can also develop pulse sequences and novel contrast mechanisms for which PMRI might have unique advantages. If our research is successful, we hope to develop a new ultra-low-cost form of high-quality MRI. Since cost is one of the key obstacles for replacing more invasive x-ray mammography, our research could have a major impact on the diagnosis and treatment of breast cancer.

References

- [1] G. Scott, S. Conolly, and A. Macovski, Noise factor bandwidth limits for high Q receiver coils, in "Abstracts of the Society of Magnetic Resonance, 3rd Annual Meeting", p. 936, Nice, Aug. 1995. Society of Magnetic Resonance.
- [2] R. Black, T. Early, P. Roemer, O. Mueller, A. Mogro-Campero, L. Turner, and G. Johnson, A high-temperature superconducting receiver for nuclear magnetic resonance microscopy, *Science*, **259**, 793-795, (1993).
- [3] S. Conolly, G. Scott, and A. Macovski, Minimum-cost solenoid design for prepolarized MRI, in "Proceedings of the ISMRM", p. 255, March 1998.
- [4] S. Conolly, R. Brown, and A. Macovski, SNR and dB/dt tradeoffs for prepolarized MRI, in "Proceedings of the Society of Magnetic Resonance", August 1995.
- [5] T. Lindstrom and S. Koenig, Magnetic-field-dependent water proton spin-lattice relaxation rates of hemoglobin solutions and whole blood, *J. Magn. Reson.*, **15**, 344-353, (1974).
- [6] R. Brooks and G. D. Chiro, Magnetic resonance imaging of stationary blood: A review, *Med. Phys.*, **8**, 903-913, (1987).
- [7] R. G. Bryant, K. Marill, C. Blackmore, and C. Francis, Magnetic relaxation in blood and blood clots, *Magn. Reson. Med.*, **13**, 133-144, (1990).
- [8] J. Gomori, R. Grossman, C. Yu-Ip, and T. Asakura, NMR relaxation times of blood: Dependence on field strength, oxidation state, and cell integrity, *Journal of Computer Assisted Tomography*, **11**(4), 684-690, (1987).
- [9] H. Fischer, P. Rinck, Y. Haverbeke, and R. Muller, Nuclear relaxation of human brain gray and white matter: Analysis of field dependence and implications for MRI, *Magn. Reson. Med.*, **16**, 317-334, (1990).
- [10] O. Henriksen, J. D. Certaines, A. Spisni, M. Cortsen, R. Muller, and P. Ring, V. in vivo field dependence of proton relaxation times in human brain, liver and skeletal muscle: A multicenter study, in "mri", volume 11, pp. 851-856, 1993.
- [11] P. Bottomley, T. Foster, R. Argersinger, and L. Pfeifer, A review of tissue hydrogen NMR relaxation times and relaxation

- mechanisms from 1-100 MHz: Dependence on tissue type, NMR frequency, temperature, species, excision, and age, *Med. Phys.*, **11**, 425-448, (1984).
- [12] R. G. Bryant, D. A. Mendelson, and C. Lester, The magnet field dependence of proton spin relaxation in tissues, *Magnetic Resonance in Medicine*, **21**, 117-126, (1991).
- [13] G. Scott, S. Conolly, P. Morgan, and A. Macovski, Low cost controller for prepolarized MRI, in "Abstracts of the Society of Magnetic Resonance, 4th Annual Meeting", p. 1386, New York, April 1996. Society of Magnetic Resonance.
- [14] G. Scott, H. Xu, S. Conolly, and A. Macovski, Single conversion image reject receiver for low field MRI, in "Abstracts of the Int. Soc. Magnetic Resonance, 5th Annual Meeting", p. 60, Vancouver, April 1997. Intl. Soc. of Magnetic Resonance.
- [15] D. B. Montgomery, "Solenoid Magnet Design". Krieger, Huntington, AL, 1980.
- [16] S. Conolly, N. I. Matter, G. Scott, and A. Macovski, A high-power pulsing circuit for prepolarized MRI, in "Proceedings of the ISMRM", p. 473, April 1999.
- [17] M. Garrett, Thick cylindrical coil systems with field or gradient homogeneities of the 6th to 20th order, *J. Appl. Phys.*, **38**(6), 2563-2586, (1967).
- [18] L. McKeethan, Combinations of circular currents for producing uniform magnetic fields., *R.S.I.*, **7**, 150-153, (1936).
- [19] P. Morgan, S. Conolly, G. Scott, and A. Macovski, A readout magnet for prepolarized MRI, *Magn. Reson. Med.*, **36**, 527-536, (Oct. 1996).
- [20] D. K. T. Claasen-Vujcic, H. Konijnenburg, J. Creighton, J. Trommel, and A. Mehlkopf, Magnet system for very low field imaging, in "Abstracts of the Soc. Magnetic Resonance, 3rd Annual Meeting", p. 933, Nice, Aug. 1995. Soc. of Magnetic Resonance.
- [21] N. O. Fenzi and S. I. Long. Low noise preamplifier. U.S. Patent 5,488,382, 1996.
- [22] G. Scott, S. Conolly, and A. Macovski, Low field preamp matching design for high Q receiver coils, in "Abstracts of the Society of Magnetic Resonance, 4th Annual Meeting", p. 396, New York, April 1996. Society of Magnetic Resonance.
- [23] M. J. Golay. Magnetic field control apparatus. U.S. Patent 3,515,979, 1957.
- [24] R. Turner, A target field approach to optimal coil design, *J. Phys. E: Scientific Instruments*, **19**, 147-151, (1986).
- [25] R. Turner, Minimum inductance coils, *J. Phys. E: Scientific Instruments*, **21**, 948-952, (1988).
- [26] R. Turner, Gradient coil design: a review of methods, *Magn. Reson. Imaging*, **11**, 903-20, (1993).
- [27] E. Wong, A. Jesmanowicz, and J. Hyde, Coil optimization for MRI by conjugate gradient descent, *Magnetic Resonance in Medicine*, **21**, 39-48, (1991).
- [28] E. Andrew and E. Szczesniak, Low inductance transverse gradient system of restricted length, *Magnetic Resonance Imaging*, **13**, 607-613, (1995).
- [29] S. Crozier and D. Doddrell, Gradient-coil design by simulated annealing, *Journal of Magnetic Resonance*, **103**, 354, (1993).
- [30] S. Crozier, L. Forbes, and D. Doddrell, The design of transverse gradient coils of restricted length by simulated annealing,

- Journal of Magnetic Resonance A*, **107**, 126, (1994).
- [31] S. Crozier and D. Doddrell, A design methodology for short whole body shielded gradient coils for MRI, *Magnetic Resonance Imaging*, **13**, 615, (1995).
- [32] H. Xu, S. Conolly, G. Scott, and A. Macovski, Gradient design with arbitrary geometrical constraints by linear programming, in "Proceedings of the ISMRM", p. 747, April 1999.
- [33] K. Foster and H. Schwan, Dielectric properties of tissues and biological materials: A critical review, *Crit. Rev. Biomed. Eng.*, **17**, 25-104, (1989).
- [34] R. Stoy, K. Foster, and H. Schwan, Dielectric properties of mammalian tissues from 0.1 to 100 MHz: a summary of recent data, *Phys. Med. Biol.*, **27**, 501-513, (1982).
- [35] D. Hoult and P. Lauterbur, The sensitivity of the zeugmatographic experiment involving human samples, *J. Magn. Reson.*, **34**, 425-433, (1979).
- [36] D. Gadian and F. Robinson, Radiofrequency losses in NMR experiments on electrically conducting samples, *J. Magn. Reson.*, **34**, 449-455, (1979).
- [37] A. C. Wright, H. K. Song, and F. W. Wehrli, In vivo MR micro imaging with conventional radiofrequency coils cooled to 77 degrees K, *Magn Res Med*, **43**, 163-169, (2000).